Superconductivity in Li-intercalated 1*T*-$SnSe_2$ driven by electric field gating

Yanpeng Song,[1,2] Xiaowei Liang,[3] Jiangang Guo,[1,4,*] Jun Deng,[1,2] Guoying Gao,[3] and Xiaolong Chen[1,2,4,†]

[1]*Beijing National Laboratory for Condensed Matter Physics, Institute of Physics, Chinese Academy of Sciences, Beijing 100190, China*

[2]*University of Chinese Academy of Sciences, Beijing 100049, China*

[3]*Center for High Pressure Science, State Key Laboratory of Metastable Materials Science and Technology, Yanshan University, Qinhuangdao 066004, China*

[4]*Songshan Lake Materials Laboratory, Dongguan, Guangdong 523808, China*

(Received 13 January 2019; revised manuscript received 1 April 2019; published 28 May 2019)

Creating carrier reservoirs in layered compounds can effectively tune the carrier density, which often induces a variety of emergent properties. Based on solid-ion-conductor gating technique, we successfully induce superconductivity of 4.8 K in ultrathin Li-intercalated $SnSe_2$ samples. The Li^+ ions are driven in between interspacing of $SnSe_2$ layers and form a single reservoir layer to provide electrons. In addition, a domelike T_c is found through substituting S for Se, where the optimal T_c is 6.2 K for $SnSe_{1.8}S_{0.2}$. Density-functional theory calculations confirm that the intercalated $LiSnSe_2$ is thermodynamically favorable, where the intercalation of Li expands the interlayer spacing by 10% and increases the carrier density by two orders of magnitude. Meanwhile, the calculated results reveal that the enhanced electron-phonon interaction due to softened phonons determines the occurrence of superconductivity. Our results demonstrate that this strategy is very effective to explore superconductors in layered materials with narrow band gaps.

DOI: 10.1103/PhysRevMaterials.3.054804

I. INTRODUCTION

Carrier tuning is essential for inducing many emergent properties such as superconductivity (SC) [1], stripe phase [2], pseudogap [3], charge density wave [4], and nematic phase [5] in cuprate and iron-based superconductors. The ways of hole doping (Ba^{2+} for La^{3+}) and electron doping (F^- for O^{2-}) in La_2O_2 layers successfully induce SC at 38 K and 26 K in La_2CuO_4 and LaFeAsO, respectively [6,7]. Other routelike exertion of chemical or physical pressure plays a similar role as chemical doping does, as manifested by induced SC in $AeFe_2As_2$ (Ae = Ca, Sr, Ba) [8–11]. The emergence of SC upon such tuning routes is related to change the curvature of energy band and geometry of Fermi surface.

For those compounds without carrier-supplying layer, creating a spacer layer in a van der Waals gap is an effective strategy for inducing SC. For example, inserting a spacer layer of K^+ and $Tl^+/Rb^+/Cs^+$ in between FeSe layers can form a $A_xFe_{2-y}Se_2$ phase (A = K, Tl, Rb, Cs) and enhance the superconducting critical temperature (T_c) in bulky FeSe from 8 K to 31 K [12–15]. It is worthy to note that the intercalation of $Na_x(NH_3)_y$ or $[Li_{0.8}Fe_{0.2}OH]^{+\sigma}$ layer into FeSe layer further increases T_c to 41–45 K, although it is not stable at elevated temperatures [16,17]. Hence, low-temperature synthesis routes like hydrothermal and solvothermal methods are conducive to obtain those superconductors [18,19]. Recently, an intercalated method through electric-field gating has been used to induce the highest T_c (48 K) in FeSe-based superconductors at ambient pressure [20–22]. The back gate applied on a solid-ion-conductor of $Li_2Al_2SiP_2TiO_{13}$ can drive the cation (Li^+) into FeSe precursor, and thus enhance carrier concentration and T_c. It provides a relatively clean process of carrier tuning without drastically altering the crystal structure of the parent compound. One thing that should be noted is that this method differs from that of ionic-liquid gating, where no ions migrate into the precursor and thus the SC is confined within surface layers (thickness of ~1 nm) [23,24].

$SnSe_2$ is an intrinsic semiconductor with a band gap of 1.0 eV at room temperature [25]. Intercalation of $Co(\eta\text{-}C_5H_5)_2$ molecules between $SnSe_2$ layers can induce SC at $T_c = 5$ K [26,27]. Besides, two-dimensional SC has been found in the interface of $SnSe_2$/ionic-liquid and $SnSe_2$/graphene [28,29]. Here, we choose ultrathin 1*T*-phase $SnSe_2$ with thickness ~13 nm as a host to testify the carrier-tuning effect on transport properties through electric-field gating. We find that a transition from semiconductor to superconductor for $SnSe_2$ is due to Li-intercalation driven by electric field. The highest T_c, 6.2 K, occurs when combining Li-intercalation and partial chemical substitution of S for Se. Theoretical calculations support that the Li ions might occupy an interlayer position to form a carrier reservoir. Within the framework of Bardeen-Cooper-Schrieffer (BCS) theory, our calculations show that electron-phonon coupling (EPC) constant (λ) is 0.97 and the phonon-mediated mechanism is responsible for SC.

II. EXPERIMENTAL

A. Experimental details

Single crystal of $SnSe_2$ was grown by chemical vapor transport method in a two-zone furnace ($T_1 = 1000$ K and $T_2 = 800$ K) with iodine as the transport agent. Selected area

*jgguo@iphy.ac.cn
†xlchen@iphy.ac.cn

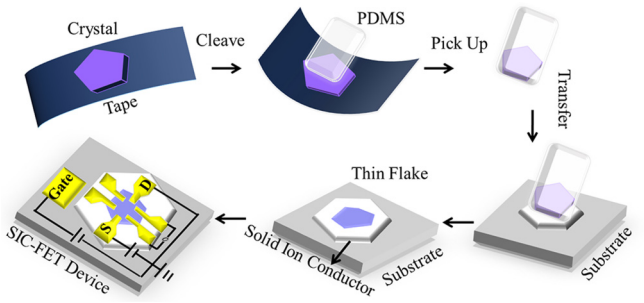

FIG. 1. Step-by-step process for fabricating $SnSe_2$/solid-ion-conductor device. Yellow electrode patterns are deposited on the surface of $SnSe_2$ and solid-ion-conductor, respectively.

electron diffraction (SAED) was carried out on a transmission electron microscopy (JEM-2100 Plus). Standard mechanical-exfoliation method with Scotch tape was used to obtain thin flakes of $SnSe_2$. A step-by-step process is illustrated in Fig. 1. We exfoliated thin flakes of $SnSe_2$ from bulk crystal by Scotch tape. The thickness of the flake was characterized by atomic force microscope (AFM) (Bruker Multimode 8). Typical samples of $10 \sim 30$ nm were transferred on a solid-ion conductor by a piece of polydimethylsiloxane. Au film of 50 nm was predeposited on the opposite surface of solid-ion conductor through electron beam evaporation. The conductor was placed on a Au-coated SiO_2/Si substrate. We then deposited Ti/Au or Cr/Ag (5/50 nm) metal electrodes with standard four-terminal and Hall-terminal patterns on $SnSe_2$ surface. The whole device was then quickly loaded into a refrigerator to avoid absorption of water or oxygen from the air. It is known that the Li-ion conductivity of solid-ion-conductor $Li_2Al_2SiP_2TiO_{13}$ (HF-Kejing) is 10^{-4} S cm^{-1} as $T > 160$ K. Thus, we slowly increased T to 160 K in case of overcharging. A lock-in amplifier (Stanford Research 830) was used to measure the transport properties. The gate voltage, $V_G = 4.5$ V, was supplied by a Keithley-2400 source meter. The resistance of $SnSe_2$ started to drop upon applying electric-field, meaning that Li ions of $Li_2Al_2SiP_2TiO_{13}$ are driven into $SnSe_2$, see Fig. S1 [30]. Meanwhile, the intercalation of Li ions is also confirmed by the I_{DS}-V_G curve as shown in Fig. S2, where the positive voltage can effectively reduce resistance and increase I_{DS}.

B. Computational details

Our calculations were based on density-functional theory (DFT) by using plane-wave pseudopotential method as implemented in the Vienna *ab initio* simulation package [31]. The electron-ion interactions were described by the projector-augmented wave potentials with $5s^25p^2$, $4s^24p^4$, and $2s^1$ configurations treated as valence electrons for Sn, Se, and Li, respectively. The exchange-correlation function was described using Perdew-Burke-Ernzerhof [32] of generalized gradient approximation. A kinetic cutoff energy of 600 eV and corresponding Monkhorst-Pack (MP) [33] k-point meshes for different structures were adopted to ensure that the enthalpy converges to 1 meV/atom. The electron-phonon interaction of $LiSnSe_2$ was calculated within the framework of linear response theory through the Quantum ESPRESSO code [34], where Norm-conserving pseudopotentials for Sn, Se, and Li with a kinetic energy cutoff of 70 Ry were employed. We adopted a $9 \times 9 \times 5$ q-point mesh and $36 \times 36 \times 20$ MP k-point mesh in the first Brillouin zone for the EPC calculations.

III. RESULTS AND DISCUSSION

$SnSe_2$ only has a 1T-type crystal structure with $a = 3.807$ Å and $c = 6.128$ Å (space group $P\bar{3}$m1), differing from the polymorphism of most transition metal dichalcogenides. Figures 2(a)–2(c) show crystal structures of $SnSe_2$ and slightly distorted $SnSe_6$ octahedron. Each Sn is surrounded by six Se with a Sn-Se bondlength of 2.88 Å and a Se-Sn-Se angle of 93°. The interlayer spacing is as large as 3.07 Å, implying that the interaction is weak Van de Waals force.

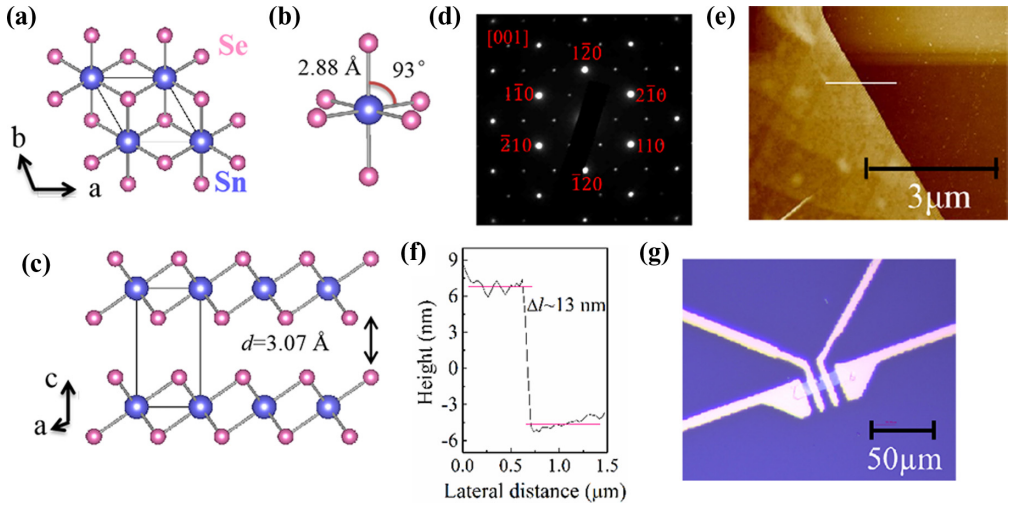

FIG. 2. (a)–(c) Crystal structure of $SnSe_2$ and $SnSe_6$ octahedron. The Sn-Se bond length, Se-Sn-Se angle, and interlayer spacing are labeled. (d) Selected area electron diffraction (SAED) of single crystal of $SnSe_2$ along [001] zone axis. (e) AFM topographic image of $SnSe_2$ thin flake. (f) Cross-sectional profile of $SnSe_2$ along the white line in (e). The thickness (Δl) is 13 nm. (g) Optical image of four electrodes on $SnSe_2$.

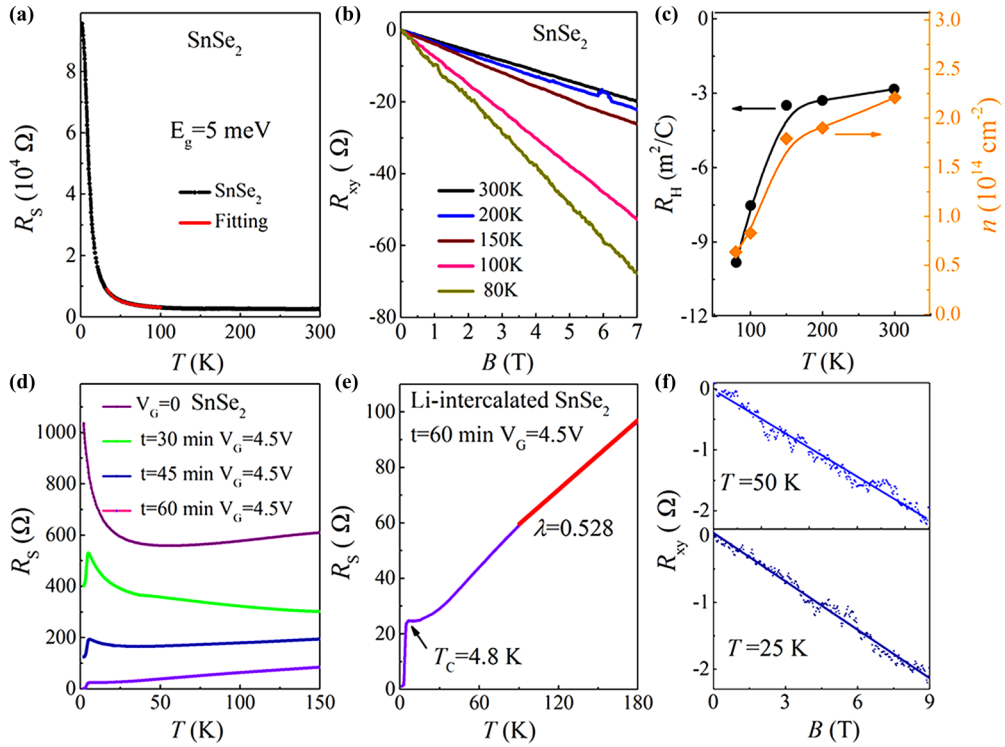

FIG. 3. (a) Temperature-dependent R_s of $SnSe_2$ thin flake without applying gating voltage. (b) Magnetic-field dependence of Hall resistance (R_{xy}) measured at 80 K, 100 K, 150 K, 200 K, and 300 K. (c) Temperature dependence of the Hall coefficient (R_H) and 2D carrier concentration (n) of $SnSe_2$. (d) Temperature-dependent R_H of Li-intercalated $SnSe_2$ between 2 K and 150 K under $V_G = 4.5$ V with different gating time (t). (e) Superconducting transition occurs at $T_c = 4.8$ K. Red line is fitting curve from 90 K to 180 K. (f) Magnetic-field dependence of R_{xy} of Li-intercalated $SnSe_2$ measured at 25 K and 50 K, respectively.

In Fig. 2(d), the SAED along [001] zone axis confirms that the as-grown single crystal has high crystallinity. From the AFM image, we can find that the exfoliated $SnSe_2$ is ~13 nm thick, i.e., 20 unit cells, as shown in Fig. 2(e) and 2(f). The optical image of the sample and four electrodes are shown in Fig. 2(g), and the transverse size of the sample is ~50 μm.

The temperature-dependent sheet electrical resistance (R_s) of $SnSe_2$ is plotted in Fig. 3(a). The curve shows the overall semiconducting character. The data in the intermediate temperature range can be fitted by equation, $R(T) = R(0)\exp[E_g/k_BT]$, where E_g is thermal-active gap, k_B the Boltzmann constant. Fitting the curve yields an $E_g = 5$ meV, which is much smaller than the band gap of bulk $SnSe_2$ (~1.0 eV). The Hall coefficient (R_H) and carrier concentration (n) of $SnSe_2$ were calculated from magnetic-field-dependent Hall resistance (R_{xy}). Based on the linear relationship between R_{xy} and magnetic field (B) up to 7 T, see Fig. 3(b), we can fit the slop and obtain the $R_H = R_{xy}/B$. The R_H is negative in the measured temperature range. Temperature-dependent R_H and n are plotted in Fig. 3(c). The R_H gradually decreases from $-3\,m^2/C$ to $-10\,m^2/C$ with decreasing temperature. Thus, the n, calculated from single-band model $n = 1/eR_H$, decreases from 2.2×10^{14} cm^{-2} to 6×10^{13} cm^{-2} from 300 K to 80 K. This value is consistent with relatively high carrier concentration in few-layer $SnSe_2$ [35], while it is higher than $10^{12} - 10^{13}$ cm^{-2} of few-layer MoS_2 and $MoSe_2$ [36,37].

To verify the effect of electric-field gating on SC, we measure the transport properties of $SnSe_2$ down to 2 K under a positive $V_G = 4.5$ eV. Figures 3(d) and 3(e) are the variation of the R_s against temperature. We found that the $SnSe_2$ changes into metal with increasing gating time (t), meaning that Li^+ driven by electric field enters into $SnSe_2$ so that Li-intercalation increases the carrier concentration. Meanwhile, a slight drop of resistance shows up at 4.8 K, and this transition gradually enhances with increasing t. From Fig. 3(e), one can find that a superconducting transition occurs at $T_c^{onset} = 4.8$ K and $T_c^{zero} = 3.5$ K, which are comparable to those T_c in $SnSe_2$-based superconductors. Here, we use the electron-phonon scattering model to analyze the λ of Li-intercalated $SnSe_2$. In the high-temperature limit ($T/\Theta_D \gg 1$, where Θ_D is the Debye temperature), the resistivity can be expressed as [38,39]

$$\rho \approx \rho_0 + \lambda \frac{2\pi m k_B}{\hbar e^2 n_0} T, \tag{1}$$

where ρ_0 is temperature-independent resistivity due to electron-impurity scattering, λ EPC constant, m effective mass, k_B the Boltzmann constant and n_0 volume carrier density. For the $SnSe_2$ sample with thickness Δl, the R_s and n are $R_s = \rho_0/\Delta l$ and $n = n_0 \times \Delta l$, respectively. Therefore,

$$R_s \approx R_0 + \lambda \frac{2\pi m k_B}{\hbar e^2 n} T = R_0 + \lambda \frac{2\pi \hbar k_B}{\varepsilon_0 \Delta l (\hbar\omega_p)^2} T, \tag{2}$$

where the bulk plasma frequency ($\hbar\omega_p$) for $SnSe_2$ is 1.01×10^5 cm^{-1} [40], ε_0 the vacuum permittivity. Fitting temperature-dependent R_s from 90 K to 180 K yields λ is 0.53. In addition, the Hall resistance R_{xy} of Li-intercalated $SnSe_2$ is measured to estimate the carrier concentration.

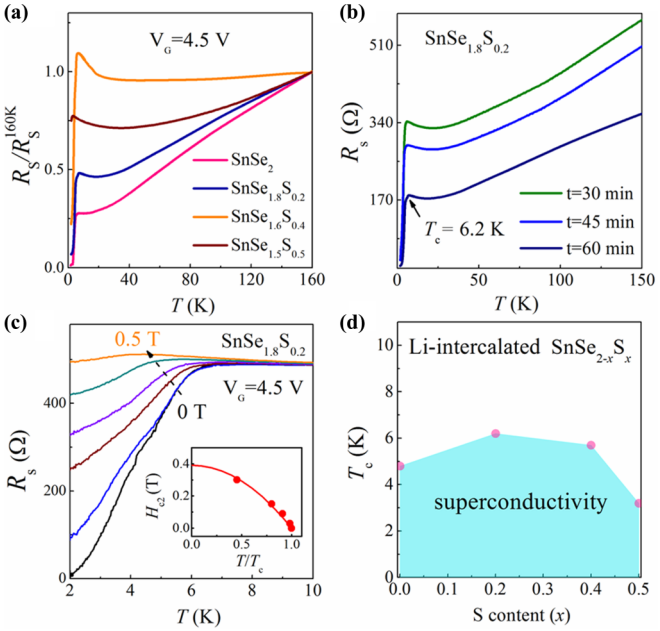

FIG. 4. (a) Superconducting transitions were observed in all $SnSe_{2-x}S_x$ ($x = 0.2,\ 0.4,\ 0.5$) samples under $V_G = 4.5$ V. (b) Temperature-dependent R_s between 2 K and 150 K of $SnSe_{1.8}S_{0.2}$ with different gating times. (c) Temperature dependence of the magnetoresistance of $SnSe_{1.8}S_{0.2}$. The inset shows the temperature dependence of H_{c2} for $SnSe_{1.8}S_{0.2}$. The red line denotes the fitting curve obtained from the Ginzburg-Landau model. (d) Superconducting phase diagram of $SnSe_{2-x}S_x$. The T_c first increases to 6.2 K at $x = 0.2$, and then it decreases as $x > 0.2$.

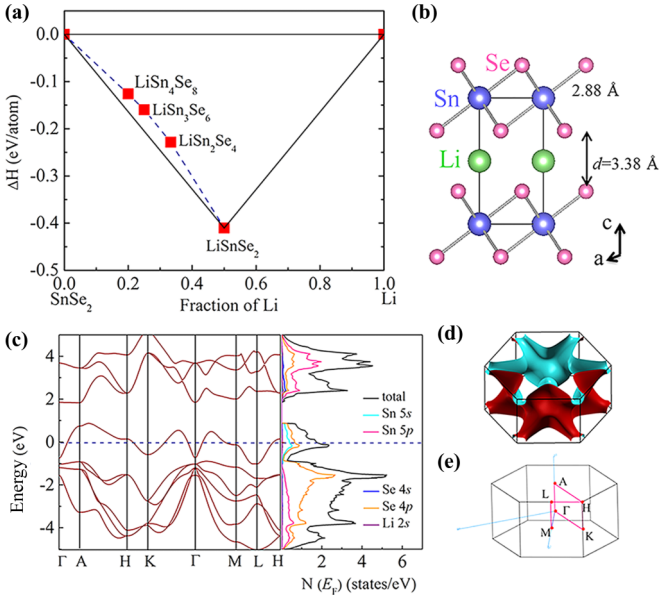

FIG. 5. (a) Relative enthalpies of formation per atom of different Li-$SnSe_2$ compositions. (b) Predicted structure of $LiSnSe_2$. (c) Band structure and projected density of states for $LiSnSe_2$. (d), (e) Fermi surface and the first Brillouin zone for $LiSnSe_2$.

The magnetic-field-dependent R_{xy} at 25 K and 50 K are plotted in Fig. 3(f). We extract R_H from the linear fitting of magnetic-field-dependent R_{xy} and calculate the $n = 1/eR_H$. It turns out that application of gate voltage, $V_G = 4.5$ V, increases the n as high as $\sim 2.58 \times 10^{15}$ cm^{-2} at $T = 25$ K.

Next, we investigate the SC of electric-field gated $SnSe_{2-x}S_x$ ($x = 0.2,\ 0.4,\ 0.5$) samples and present the data in Fig. 4. Similar superconducting transitions were also observed in $SnSe_{2-x}S_x$ ($x = 0.2,\ 0.4,\ 0.5$) under the same $V_G = 4.5$ eV, as shown in Fig. 4(a). Figure 4(b) shows that the resistivity gradually decrease with increasing gating time, and the optimal transition can be reached as t= 60 min. The temperature-dependent R_s of $SnSe_{1.8}S_{0.2}$ under varying perpendicular magnetic fields is shown in Fig. 4(c). It can be seen that the superconducting transition gradually broadens and the T_c shifts to lower temperatures as the magnetic field increases. Meanwhile, as a criteria of 90% of the normal state resistance, we plotted the temperature dependence of the field H_{c2} for Li-intercalated $SnSe_{1.8}S_{0.2}$ in the inset of Fig. 4(c). These data can be fitted by the Ginzburg-Landau equation $H_{c2} = H_{c2}(0)[1 - (\frac{T}{T_c})^2]$ and the obtained $H_{c2}(0) = 0.39$ T. Using the equation of $H_{c2}(0) = \frac{\Phi_0}{2\pi\xi_{GL}(0)^2}$, where Φ_0 is the magnetic flux quantum (2.07×10^{-15} Wb), we obtained the $\xi_{GL}(0) = 29$ nm. A superconducting phase diagram of T_c versus S content is plotted in Fig. 4(d). In the $SnSe_{2-x}S_x$ sample ($x \leqslant 0.5$), an interesting point is that the T_c^{onset} first increases to 6.2 K at $x = 0.2$, and then it begins to decrease as $x > 0.2$. It is known that the S substitution can induce contraction of lattice constants and Sn-Se/S bond length, which generates the effect of chemical pressure without introducing extra electrons [41]. As for the S-substitution effect on SC, we think that it is similar with the observations in $FeSe_{1-x}S_x$, in which the T_c^{onset} first increases and then decreases with increasing S, and the maximal T_c^{onset} emerges at 20% S-substitution. This enhancement T_c^{onset} should be related to the optimized Fe-Se bond length and geometry of $FeSe_4$ tetrahedra [42]. Another possibility is that the substitution of S for Se results in a greater orbital overlap, increasing the bandwidth and driving the system more itinerant [43]. In the S-rich $SnSe_{2-x}S_x$ sample (x > 0.5), the R_s is too large to be measured [44]. The electric-field gating is hard to metallize this sample and induce SC. We notice that, in all samples, the T_c^{onset} does not increase with increasing t. It implies that there is only one superconducting phase, which is different from multiple phases in intercalated FeSe-based superconductors [22,45,46].

To better understand the effect of Li-intercalation on the structure and SC of $SnSe_2$, the DFT calculations were performed. Here, four stoichiometries of Li-intercalated phases, $LiSnSe_2$, $LiSn_2Se_4$, $LiSn_3Se_6$, and $LiSn_4Se_8$, were adopted to simulate different Li concentrations. Their crystal structures were constructed based on the $P\bar{3}m1$ space group, where one Li atom occupies one octahedral interstice surrounding by six Se atoms (Wyckoff position of $P\bar{3}m1$: 1b) in $1 \times 1 \times 1$, $1 \times 1 \times 2$, $1 \times 1 \times 3$, and $2 \times 2 \times 1$ supercells of $LiSnSe_2$, respectively. We first investigate the phase stability of Li-intercalated $SnSe_2$ by calculating their formation enthalpies relative to Li and binary $SnSe_2$, where the most stable structures for Li and $SnSe_2$ at ambient pressure were adopted [47]. As shown in Fig. 5(a), all the stoichiometries have negative formation enthalpies relative to Li and $SnSe_2$, suggesting that the intercalation of Li is thermodynamically

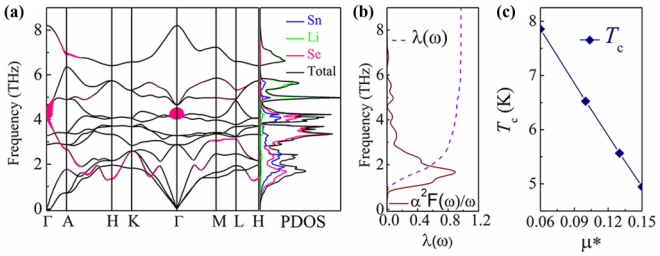

FIG. 6. (a) Calculated phonon spectra and PDOS. Magenta solid circles show the phonon linewidth with a radius proportional to the EPC strength. (b) Eliashberg spectral function $\alpha^2F(\omega)/\omega$ and EPC constant (λ) as a function of frequency. (c) Coulomb repulsion constant μ^* dependence of T_c.

favored. With increasing Li content, the formation enthalpies monotonously decrease and $LiSnSe_2$ achieves the lowest one, -0.42 eV/atom, indicating that it is the most stable compound. In addition, the formation enthalpies of $LiSn_2Se_4$, $LiSn_3Se_6$, and $LiSn_4Se_8$ lying above the convex hull suggest that they are unstable with respect to decomposition into $LiSnSe_2$ and $SnSe_2$. The obtained crystal structure of $LiSnSe_2$ is shown in Fig. 5(b), where $a = 3.955$ Å and $c = 6.751$ Å. The Li ions intercalate into interlayer of $SnSe_2$ and form a carrier-supply reservoir. The interlayer spacing is expanded to 3.38 Å after Li interaction, but the Sn-Se bond length is still 2.88 Å. The calculated electronic band structure and projected density of states (DOS) for $LiSnSe_2$ are shown in Fig. 5(c). Comparing with the band structure of semiconducting $SnSe_2$ in Fig. S3 and Ref. [48], doping of one Li^+ seems to upshift the Fermi level (E_F) by $\sim$1 eV. One can see that a single band crosses the E_F from -1 eV to 1 eV, indicative of metallic behavior, which is consistent with the experimental result. The electronic DOS at E_F is 2.1 states/eV, which is dominated by Sn 5s and Se 4p orbitals with strong hybridization. The contribution of Se 4p is a little larger than that of Sn 5s. From the calculated Fermi surface of $LiSnSe_2$, shown in Figs. 5(d) and 5(e), we can see that a three-dimensional-like characteristic in electronic structure appears. There is a small electron pocket at Γ point of the first Brillouin zone.

The calculated phonon spectra for $LiSnSe_2$ are plotted in the left panel of Fig. 6(a). There is no imaginary frequency in the full spectrum, indicating that it is dynamically stable. The corresponding projected phonon DOS (PDOS) is shown in the right panel of Fig. 6(a). It can be seen that the low-frequency bands below 4 THz are dominated by Sn and Se states, while the high frequency modes above 5 THz mainly comes from Li vibrations. In comparison with the phonon spectra and PDOS for $SnSe_2$, see Figs. S3(b) and S3(d), the intercalation of Li drives the partial phonon modes below 4 THz move to low-frequency range and enhances the peak at 2 THz. It can induce phonon softening, which enhances the EPC and facilitates SC. To explore the SC of $LiSnSe_2$, the Eliashberg spectral function $\alpha^2F(\omega)$ and the λ are calculated as shown in Fig. 6(b). The spectra function $\alpha^2F(\omega)$ is calculated in terms of the phonon line width γ_{qj} due to electron-phonon interaction,

$$\alpha^2F(\omega) = \frac{1}{2\pi N(E_f)} \Sigma_{qj} \frac{\gamma_{qj}}{\omega_{qj}} \delta(\omega - \omega_{qj}) \omega(q), \qquad (3)$$

where $\omega(q)$ is the weight of a $\boldsymbol{q}$ point in the first BZ and $N(E_F)$ is the electronic DOS per atom and spin at the E_F. The line width of a phonon mode, γ_{qj}, can be expressed as

$$\gamma_{qj} = 2\pi\omega_{qj}\Sigma_{nm} \int \frac{d^3k}{\Omega_{BZ}} \left|g^j_{kn,k+qm}\right|^2 \delta(\varepsilon_{kn})\delta(\varepsilon_{k+qm}), \qquad (4)$$

where Ω_{BZ} is the volume of the BZ, the sum is over the first Brillouin zone, and ε_{kn} are the energies of bands measured with respect to the E_F at point k. The $g^j_{kn,k+qm}$ is the electron-phonon matrix element. The λ is thus defined as integration of the spectra function in the first Brillouin zone as the formula $\lambda = 2\int_0^\infty \frac{\alpha^2F(\omega)}{\omega} d\omega$. Besides the modes at about 4 THz at Γ point, the modes between 1–2 THz at H point and along $K - \Gamma$ direction soften, which lead to large γ_{qj} values. Accordingly, it is clearly seen that a pronounced peak shows up at 1.5 THz in the $\alpha^2F(\omega)/\omega$ curve. The calculated λ for $LiSnSe_2$ is 0.97, which mainly comes from the vibrations of Sn and Se atoms below 2 THz. Therefore, the main effect of Li intercalation is believed to not only provide carriers for $SnSe_2$ layers but also enhance the EPC.

We use the Allen-Dynes formula [49],

$$\omega_{ln} = \exp\left[\frac{2}{\lambda}\int \frac{\alpha^2F(\omega)}{\omega} \ln\omega\, d\omega\right], \qquad (5)$$

$$k_BT_c = \frac{\hbar\omega_{ln}}{1.2} \exp\left[-\frac{1.04(1+\lambda)}{\lambda - \mu^*(1+0.62\lambda)}\right], \qquad (6)$$

to accurately evaluate the T_c, where ω_{ln} is the logarithmic average of the phonon frequencies, μ^* is the Coulomb repulsion constant. The ω_{ln} is calculated to be 98.2 K, which is significantly softened by 40% compared with the Debye temperature of bulk $SnSe_2$ (140 ± 2 K) [50]. The μ^* dependence of T_c is plotted in Fig. 6(c). The calculated T_c linearly decreases from 7.8 K to 4.8 K as increasing μ^*. Taking the common value of the μ^* as 0.13, the theoretical T_c of $LiSnSe_2$ is 5.5 K. Notably, the theoretical T_c is consistent with the experimental one, indicating that the SC of $LiSnSe_2$ can be well described by the phonon-mediated mechanism.

Like enhancing SC of binary FeSe through external pressure, squeezing $SnSe_2$ can optimize the structure and carrier concentration, and then induce SC. In pressurized $SnSe_2$, the possibility of phase decomposition due to structural instability could soften the partial phonon modes, which enhances the EPC [51]. In Li-intercalated $SnSe_2$, the newly formed carrier layers can induce two kinds of effects. One is leading to phonon softening of $SnSe_2$, which could enhance the EPC and induce the SC according to the BCS theory. The other is that creating the carrier layer of Li^+ transfers electrons into the $SnSe_2$ layer and realizes intrinsically heavily doped $SnSe_2$ [26,27]. Our electric-field gating can increase carrier concentration by one or two orders of magnitude. The $SnSe_2$ with high carrier density has been demonstrated to be superconductors with $T_c = 3.9$ K [28] and 4.8 K [29]. However, we noticed that this gating method may not change the compound with large band gap (>2 eV) into metal, and the tuning ability is limited under these circumstances. Designing new devices, such as electric-double-layer transistor with liquid and solid ions, could further induce more superconductors from metal chalcogenides with large band gaps.

IV. CONCLUSION

In summary, we report a semiconductor-superconductor transition of 4.8 K in Li-intercalated $SnSe_2$ through electric-field gating. A maximal T_c of 6.2 K is obtained by optimizing the gating time and chemical substitution of S for Se. More importantly, theoretical calculations reasonably predict the intercalated crystal structure and the metallic behaviors of $LiSnSe_2$. Besides, the partial phonon softening due to Li-intercalation strengthens the EPC, leading to the occurrence of SC. The combinations of experimental and theoretical results demonstrate that this method is highly effective for increasing carrier concentration and metallizing layered materials. Meanwhile, it is useful to study the intrinsic properties of superconducting layers because Li-intercalation of this method can keep the crystal structure intact to a larger extent.

ACKNOWLEDGMENTS

This work is financially supported by the National Natural Science Foundation of China (No. 51772322, No. 51532010, No. 11604290, and No. 51732010), by the National Key Research and Development Program of China (No. 2016YFA0300600 and No. 2017YFA0304700), by the Chinese Academy of Sciences under Grant No. QYZDJ-SSW-SLH013, the Funding Program for Recruited Oversea Scholars of Hebei Province (CL201729), and the Ph.D. foundation by Yanshan University (Grant No. B970).

[1] M. Imada, A. Fujimori, and Y. Tokura, Rev. Mod. Phys. **70**, 1039 (1998).
[2] J. M. Tranquada, B. J. Sternlieb, J. D. Axe, Y. Nakamura, and S. Uchida, Nature (London) **375**, 561 (1995).
[3] H. Ding, T. Yokoya, J. C. Campuzano, T. Takahashi, M. Randeria, M. R. Norman, T. Mochiku, K. Kadowaki, and J. Giapintzakis, Nature (London) **382**, 51 (1996).
[4] W. L. McMillan, Phys. Rev. B **14**, 1496 (1976).
[5] L. J. Yu and A. Saupe, Phys. Rev. Lett. **45**, 1000 (1980).
[6] P. W. Anderson, Science **235**, 1196 (1987).
[7] Y. Kamihara, T. Watanabe, M. Hirano, and H. Hosono, J. Am. Chem. Soc. **130**, 3296 (2008).
[8] E. Colombier, S. L. Bud'ko, N. Ni, and P. C. Canfield, Phys. Rev. B **79**, 224518 (2009).
[9] B. Lv, L. Deng, M. Gooch, F. Wei, Y. Sun, J. K. Meen, Y. Y. Xue, B. Lorenz, and C. W. Chu, Proc. Natl. Acad. Sci. USA **108**, 15705 (2011).
[10] M. Gooch, B. Lv, B. Lorenz, A. M. Guloy, and C.-W. Chu, Phys. Rev. B **78**, 180508(R) (2008).
[11] T. Katase, S. Iimura, H. Hiramatsu, T. Kamiya, and H. Hosono, Phys. Rev. B **85**, 140516(R) (2012).
[12] J. Guo, S. Jin, G. Wang, S. Wang, K. Zhu, T. Zhou, M. He, and X. Chen, Phys. Rev. B **82**, 180520(R) (2010).
[13] M.-H. Fang, H.-D. Wang, C.-H. Dong, Z.-J. Li, C.-M. Feng, J. Chen, and H. Q. Yuan, Europhys. Lett. **94**, 27009 (2011).
[14] A. F. Wang, J. J. Ying, Y. J. Yan, R. H. Liu, X. G. Luo, Z. Y. Li, X. F. Wang, M. Zhang, G. J. Ye, P. Cheng, Z. J. Xiang, and X. H. Chen, Phys. Rev. B **83**, 060512(R) (2011).
[15] A. Krzton-Maziopa, Z. Shermadini, E. Pomjakushina, V. Pomjakushin, M. Bendele, A. Amato, R. Khasanov, H. Luetkens, and K. Conder, J. Phys. Condens. Matter **23**, 052203 (2011).
[16] T. P. Ying, X. L. Chen, G. Wang, S. F. Jin, T. T. Zhou, X. F. Lai, H. Zhang, and W. Y. Wang, Sci. Rep. **2**, 426 (2012).
[17] L. Sun, X.-J. Chen, J. Guo, P. Gao, Q.-Z. Huang, H. Wang, M. Fang, X. Chen, G. Chen, Q. Wu, C. Zhang, D. Gu, X. Dong, L. Wang, K. Yang, A. Li, X. Dai, H.-k. Mao, and Z. Zhao, Nature (London) **483**, 67 (2012).
[18] S. Jin, X. Fan, X. Wu, R. Sun, H. Wu, Q. Huang, C. Shi, X. Xi, Z. Li, and X. Chen, Chem. Commun. **53**, 9729 (2017).
[19] R. J. Sun, Y. Quan, S. F. Jin, Q. Z. Huang, H. Wu, L. Zhao, L. Gu, Z. P. Yin, and X. L. Chen, Phys. Rev. B **98**, 214508 (2018).
[20] B. Lei, J. H. Cui, Z. J. Xiang, C. Shang, N. Z. Wang, G. J. Ye, X. G. Luo, T. Wu, Z. Sun, and X. H. Chen, Phys. Rev. Lett. **116**, 077002 (2016).
[21] B. Lei, N. Z. Wang, C. Shang, F. B. Meng, L. K. Ma, X. G. Luo, T. Wu, Z. Sun, Y. Wang, Z. Jiang, B. H. Mao, Z. Liu, Y. J. Yu, Y. B. Zhang, and X. H. Chen, Phys. Rev. B **95**, 020503(R) (2017).
[22] T. P. Ying, M. X. Wang, X. X. Wu, Z. Y. Zhao, Z. Z. Zhang, B. Q. Song, Y. C. Li, B. Lei, Q. Li, Y. Yu, E. J. Cheng, Z. H. An, Y. Zhang, X. Y. Jia, W. Yang, X. H. Chen, and S. Y. Li, Phys. Rev. Lett. **121**, 207003 (2018).
[23] K. Ueno, S. Nakamura, H. Shimotani, A. Ohtomo, N. Kimura, T. Nojima, H. Aoki, Y. Iwasa, and M. Kawasaki, Nat. Mater. **7**, 855 (2008).
[24] J. T. Ye, S. Inoue, K. Kobayashi, Y. Kasahara, H. T. Yuan, H. Shimotani, and Y. Iwasa, Nat. Mater. **9**, 125 (2009).
[25] V. Bhatt, K. Gireesan, and G. Pandya, J. Cryst. Growth **96**, 649 (1989).
[26] D. O'Hare, H.-V. Wong, S. Hazell, and J. W. Hodby, Adv. Mater. **4**, 658 (1992).
[27] Z. Li, Y. Zhao, K. Mu, H. Shan, Y. Guo, J. Wu, Y. Su, Q. Wu, Z. Sun, A. Zhao, X. Cui, C. Wu, and Y. Xie, J. Am. Chem. Soc. **139**, 16398 (2017).
[28] J. Zeng, E. Liu, Y. Fu, Z. Chen, C. Pan, C. Wang, M. Wang, Y. Wang, K. Xu, S. Cai, X. Yan, Y. Wang, X. Liu, P. Wang, S.-J. Liang, Y. Cui, H. Y. Hwang, H. Yuan, and F. Miao, Nano Lett. **18**, 1410 (2018).
[29] Y.-M. Zhang, J.-Q. Fan, W.-L. Wang, D. Zhang, L. Wang, W. Li, K. He, C.-L. Song, X.-C. Ma, and Q.-K. Xue, Phys. Rev. B **98**, 220508(R) (2018).
[30] See Supplemental Material at http://link.aps.org/supplemental/10.1103/PhysRevMaterials.3.054804 for the temperature dependence of the sheet resistance, the voltage dependence of source-drain current, and additional DTF results.
[31] G. Kresse and J. Furthmüller, Phys. Rev. B **54**, 11169 (1996).
[32] G. Kresse and D. Joubert, Phys. Rev. B **59**, 1758 (1999).
[33] H. J. Monkhorst and J. D. Pack, Phys. Rev. B **13**, 5188 (1976).
[34] P. Giannozzi, S. Baroni, N. Bonini, M. Calandra, R. Car, C. Cavazzoni, D. Ceresoli, G. L. Chiarotti, M. Cococcioni, I. Dabo, A. D. Corso, S. de Gironcoli, S. Fabris, G. Fratesi, R. Gebauer, U. Gerstmann, C. Gougoussis, A. Kokalj, M.

Lazzeri, L. Martin-Samos, N. Marzari, F. Mauri, R. Mazzarello, S. Paolini, A. Pasquarello, L. Paulatto, C. Sbraccia, S. Scandolo, G. Sclauzero, A. P. Seitsonen, A. Smogunov, P. Umari, and R. M. Wentzcovitch, J. Phys. Condens. Matter **21**, 395502 (2009).

[35] K. Ito, K. Nishikawa, and H. Iizuka, Appl. Phys. Lett. **108**, 053507 (2016).

[36] J. T. Ye, Y. J. Zhang, R. Akashi, M. S. Bahramy, R. Arita, and Y. Iwasa, Science **338**, 1193 (2012).

[37] W. Shi, J. Ye, Y. Zhang, R. Suzuki, M. Yoshida, J. Miyazaki, N. Inoue, Y. Saito, and Y. Iwasa, Sci. Rep. **5**, 12534 (2015).

[38] G. Grimvall, *The Electron-Phonon Interaction in Metals* (North-Holland Publishing Co., Amsterdam, 1981).

[39] X. Xi, H. Berger, L. Forró, J. Shan, and K. F. Mak, Phys. Rev. Lett. **117**, 106801 (2016).

[40] A. Sengupta, arXiv:1811.09031.

[41] T. S. Pan, D. De, J. Manongdo, A. M. Guloy, V. G. Hadjiev, Y. Lin, and H. B. Peng, Appl. Phys. Lett. **103**, 093108 (2013).

[42] K. Matsuura, Y. Mizukami, Y. Arai, Y. Sugimura, N. Maejima, A. Machida, T. Watanuki, T. Fukuda, T. Yajima, Z. Hiroi, K. Y. Yip, Y. C. Chan, Q. Niu, S. Hosoi, K. Ishida, K. Mukasa, S. Kasahara, J. G. Cheng, S. K. Goh, Y. Matsuda, Y. Uwatoko, and T. Shibauchi, Nat. Commun. **8**, 1143 (2017).

[43] M. D. Watson, T. K. Kim, A. A. Haghighirad, S. F. Blake, N. R. Davies, M. Hoesch, T. Wolf, and A. I. Coldea, Phys. Rev. B **92**, 121108(R) (2015).

[44] L. A. Burton, D. Colombara, R. D. Abellon, F. C. Grozema, L. M. Peter, T. J. Savenije, G. Dennler, and A. Walsh, Chem. Mater. **25**, 4908 (2013).

[45] J. Guo, H. Lei, F. Hayashi, and H. Hosono, Nat. Commun. **5**, 4756 (2014).

[46] T. Kajita, T. Kawamata, T. Noji, T. Hatakeda, M. Kato, Y. Koike, and T. Itoh, Physica C **519**, 104 (2015).

[47] G. Gao, R. Hoffmann, N. W. Ashcroft, H. Liu, A. Bergara, and Y. Ma, Phys. Rev. B **88**, 184104 (2013).

[48] J. M. Gonzalez and I. I. Oleynik, Phys. Rev. B **94**, 125443 (2016).

[49] P. B. Allen and R. C. Dynes, Phys. Rev. B **12**, 905 (1975).

[50] R. Lagnier, C. Ayache, J.-Y. Harbec, S. Jandl, and J.-P. Jay-Gerin, Solid State Commun. **48**, 65 (1983).

[51] Y. Zhou, B. Zhang, X. Chen, C. Gu, C. An, Y. Zhou, K. Cai, Y. Yuan, C. Chen, H. Wu, R. Zhang, C. Park, Y. Xiong, X. Zhang, K. Wang, and Z. Yang, Adv. Electron. Mater. **4**, 1800155 (2018).